Influence of surface excitations on electrons elastically backscattered from copper and silver surfaces

Y. F. Chen, P. Su, and C. M. Kwei
Department of Electronics Engineering, National Chiao Tung University, Hsinchu, Taiwan, Republic of China

C. J. Tung
Department of Nuclear Science, National Tsing Hua University, Hsinchu, Taiwan, Republic of China
(Received 15 April 1994; revised manuscript received 20 July 1994)

The influence of surface excitations on electrons elastically backscattered from solid surfaces is investigated. Elastic-scattering differential cross sections are calculated using the partial-wave expansion method and the finite difference techique for solid atoms with the Hartree-Fock-Wigner-Seitz potential. An extended Drude dielectric function which allows the characteristic oscillator strength, damping constant, and critical-point energy for each subband of valence electrons is employed to estimate electron inelastic mean free paths for volume excitations. The same dielectric function is applied to evaluate the probability of surface excitations for incident and escape electrons by including the recoil effect without the small-angle approximation. Results of Monte Carlo simulations on the elastic reflection coefficient and the angular distribution of electrons elastically backscattered from Cu and Ag surfaces are presented. It is revealed that surface excitations significantly reduce the elastic reflection coefficient for low-energy electrons, but less significantly influence the angular distribution for large escape angles. Our results agree very well with experimental data.

I. INTRODUCTION

The elastic peak in the spectrum of electrons escaped from solid surfaces provides important information for applications in a number of experimental techniques such as scanning electron microscopy (SEM), quantitative Auger electron spectroscopy (AES), and disappearance potential spectroscopy (DAPS), etc.[1,2] The elastic peak electron spectroscopy (EPES) has gained much attention due to the development of surface-sensitive electron spectroscopies.[3–10] In the reflection electron-energy-loss spectroscopy (REELS), angular and energy distributions of electrons backscattered from solid surfaces are analyzed to extract electron interaction cross sections.[11–13] The elastic or zero-energy-loss peak in the REELS spectrum simplifies this analysis.

Monte Carlo (MC) simulations are most widely used by a theoretical investigation of the EPES. The basic inputs required in MC simulations are the elastic scattering differential cross section, the inelastic mean free path (IMFP) of electrons for volume excitations, and the probability of surface excitations by incident and escape electrons. A few MC simulations have been applied to compute the elastic reflection coefficient and the angular distribution of elastically backscattered electrons.[14–17] These works made use of elastic-scattering differential cross sections determined from a Thomas-Fermi-Dirac (TFD) potential for free atoms.[18] IMFP's were established using an electron gas statistical model,[19,20] whereas the probability of surface excitations was omitted. A recent study on the REELS spectra,[13] however, has demonstrated that surface excitations were important for low-energy electrons. This suggests that surface excitations might also be important for the properties of elastically backscattered electrons.

In this work, we have applied the partial-wave expansion method and the finite difference technique to calculate electron elastic scattering cross sections using the Hartree-Fock-Wigner-Seitz (HFWS) solid atomic potential. Applying an extended Drude dielectric function for the valence band of solids,[21–23] we have estimated electron IMFP's for volume excitations and the probability of surface excitations by incident and backscattered electrons. Parameters in the model dielectric function were determined by a fit of this function to the optical data and by a check of the fitting results through sum rules. The probability of surface excitations by electrons obliquely passing through solid surfaces was derived including the recoil effect without the small-angle assumption. MC simulations were then performed to compute the elastic reflection coefficient and the angular distribution of electrons elastically backscattered from Cu and Ag surfaces. Results of these computations revealed that the influence of surface excitations on the elastic reflection coefficient was quite significant for low-energy electrons. This influence on the angular distribution, however, was less significant and only important for glancing escape electrons. Our results are in good agreement with experimental data.

II. MONTE CARLO SIMULATIONS

Elastic and inelastic scatterings result in zig-zag trajectories of the transport electrons in a solid; see Fig. 1(a). Elastic scatterings alter the path lengths of electrons and cause angular deflections. Inelastic interactions, on the other hand, are responsible for the energy losses of electrons. MC simulations of elastically backscattered electrons from a solid surface are straightforward. The computer keeps track of electrons inside the solid by record-

ing their trajectories in terms of the path lengths and the azimuthal and polar angles after each elastic scatterings. The probability density function of electrons scattered into the polar angle θ after an elastic scattering is determined by

$$P(\theta)=\frac{2\pi\sin\theta}{\sigma_e}\frac{d\sigma_e}{d\Omega}\ , \tag{1}$$

where $d\sigma_e/d\Omega$ is the elastic-scattering differential cross section and

$$\sigma_e=\int\frac{d\sigma_e}{d\Omega}d\Omega \tag{2}$$

is the elastic-scattering total cross section. Note that all quantities and expressions in this paper are in atomic units unless otherwise specified. Assuming a Poisson stochastic process for elastic scattering events, the probability density function of electrons traversing a path length s between two consecutive elastic scatterings is given by[24]

$$P(s)=\frac{1}{\lambda_e}\exp\left[-\frac{s}{\lambda_e}\right]\ , \tag{3}$$

where the elastic mean free path of electrons is determined from[25]

$$\lambda_e=(N\sigma_e)^{-1}\ , \tag{4}$$

and N is the atomic density of solids. It is assumed that the azimuthal-scattering angle is cylindrical symmetric.

The tracking of electrons continues until they backscattered from the solid surface or their path lengths in the solid become so large that any attainable contribution to the backscattered electron intensity can be neglected. The elastic reflection coefficient can then be calculated from

$$\eta_e(\alpha_R^{\min},\alpha_R^{\max})=\frac{1}{m}\sum_{j=1}^{m}\Delta I_j\ , \tag{5}$$

where $\alpha_R^{\min}$ and $\alpha_R^{\max}$ are the minimum and maximum values of acceptance escape angles determined by the reflected electron analyzer, m is the total number of simulated trajectories within the acceptance angles, and ΔI_j is the intensity of elastically backscattered electrons contributed by the jth trajectory within these angles. It is understood that

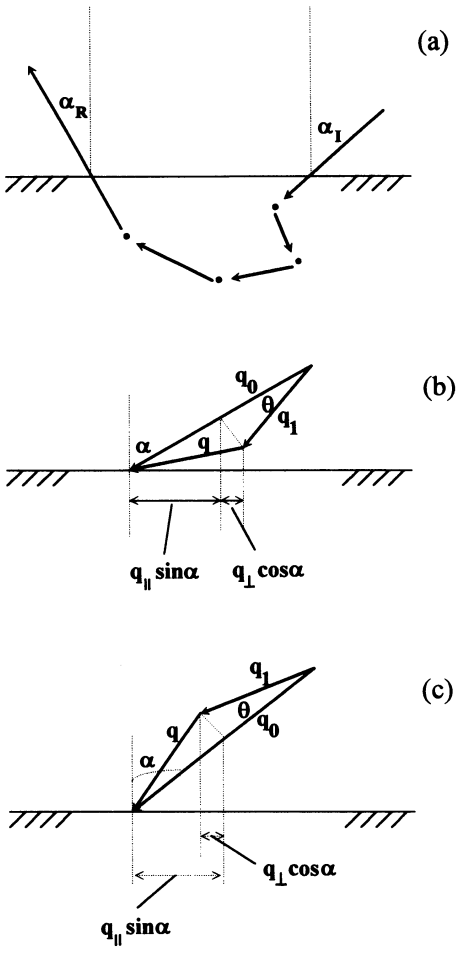

FIG. 1. (a) A sketch of the zig-zag trajectory of an elastically backscattered electron from a solid surface. (b) A vector diagram for the excitation of a surface plasmon. Here $\mathbf{q}_0$, $\mathbf{q}_1$, and $\mathbf{q}$ are, respectively, the electron momentum before scattering, the electron momentum after scattering, and the momentum transfer; $q_\parallel$ and $q_\perp$ are, respectively, the perpendicular and parallel components of $\mathbf{q}$ along $\mathbf{q}_0$; α and θ are, respectively, the angle between electron velocity and solid surface normal and the scattering angle (positive sign). The scattering is assumed to lie on the plane of incidence. (c) A vector diagram similar to (b), but with a negative scattering angle.

$$\Delta I_j=\begin{cases}\exp[-P_s(\alpha_{Ij},E)]\exp[-P_s(\alpha_{Rj},E)]\exp(-s_j/\lambda_i) & \text{if the electron leaves the solid within acceptance angles}\ ,\\ 0 \quad \text{otherwise}\end{cases} \tag{6}$$

where s_j is the path length of the jth trajectory, λ_i is the inelastic mean free path, and α_{Ij} and α_{Rj} are the angles between electron velocity and solid surface normal for incident and backscattered electrons; see Fig. 1(a). The factors $\exp[-P_s(\alpha_{Ij},E)]$ and $\exp[-P_S(\alpha_{Rj},E)]$ are the probabilities that incident and backscattered electrons cross the surface without surface excitations. The factor $\exp(-s_j/\lambda_i)$ represents the probability that the jth electron traverses a pathlength s_j inside the solid without volume excitations. While the attenuation of elastically backscattered electron follows the exponential relation for their intensity, a detailed description about inelastic processes in the interior of the solid should be considered in REELS. It is noticed that Jablonski and coworkers[14–17] have neglected the surface excitation effect by adopting the relation $\Delta I_j=\exp(-s_j/\lambda_i)$.

III. INTERACTION CROSS SECTIONS

A. Elastic scatterings

Since electron energies of interest in this work are ~100–2000 eV, the Born approximation is not adequate. Instead, the phase-shift method should be applied to calculate elastic-scattering differential cross sections. The radial wave function describing electrons of kinetic energy $E=k^2/2$ satisfies

$$\frac{d^2R_l}{dr^2}+\frac{2}{r}\frac{dR_l}{dr}+\left[k^2-2V(r)-\frac{l(l+1)}{r^2}\right]R_l=0\ , \tag{7}$$

where the scattering potential in solids may be determined from

$$V(r)=\begin{cases}-\dfrac{Z}{r}+\dfrac{1}{r}\displaystyle\int_0^r 4\pi r'^2\rho(r')dr'+\int_r^{R_{\rm WS}}4\pi r'\rho(r')dr' & \text{for } r\le R_{\rm WS}\\ 0 \quad \text{otherwise,}\end{cases} \tag{8}$$

Z is the atomic number, $\rho(r)$ is the HFWS electron density distribution of solid atoms,[26] and $R_{\rm WS}$ is the Wigner-Seitz radius.

Since the potential of Eq. (8) has a finite range in radial distance, we can divide the space into an internal region ($r<R_{\rm WS}$) and an external region ($r>R_{\rm WS}$). The solution of Eq. (7) in the external region may be given by[27]

$$R_l(r)\propto[j_l(kr)-\tan\delta_l n_l(kr)]\ , \tag{9}$$

where j_l and n_l are the spherical Bessel functions and δ_l is the phase shift of lth partial wave. In the internal region, we can apply the finite difference method to obtain a solution. We let derivatives of the radial wave function be

$$\left.\frac{dR_l}{dr}\right|_{r=r_i}=\frac{R_l(r_{i+1})-R_l(r_{i-1})}{r_{i+1}-r_{i-1}} \tag{10}$$

and

$$\left.\frac{d^2R_l}{dr^2}\right|_{r=r_i}=2\left[\frac{R_l(r_{i+1})-R_l(r_i)}{r_{i+1}-r_i}-\frac{R_l(r_i)-R_l(r_{i-1})}{r_i-r_{i-1}}\right]\Big/(r_{i+1}-r_{i-1})\ , \tag{11}$$

where $i=1,2,3,\ldots$. Substituting Eqs. (10) and (11) into Eq. (7), we find

$$R_l(r_{i+1})=\frac{r_iR_l(r_i)}{r_{i+1}}+\left[1-\frac{r_i}{r_{i+1}}\right]\left\{\frac{r_iR_l(r_i)-r_{i-1}R_l(r_{i-1})}{r_i-r_{i-1}}-\frac{r_{i+1}-r_{i-1}}{2}\left[2[E-V(r_i)]-\frac{l(l+1)}{r_i^2}\right]r_iR_l(r_i)\right\}\ . \tag{12}$$

The computations using Eq. (12) can be started by applying the initial condition: $R_l(r)=r^l$ as $r\to 0$. These computations are rapid due to the finite range in radial distance.

Defining the logarithmic derivative of the internal solution at $r=R_{\rm WS}$ as

$$\chi_l=[R_l^{-1}(dR_l/dr)]_{r=R_{\rm WS}}\ , \tag{13}$$

we obtain by applying the boundary condition, i.e., $R_l^{-1}(dR_l/dr)$ must be continuous at $r=R_{\rm WS}$,[27]

$$\chi_l=\frac{k[j_l'(kR_{\rm WS})-\tan\delta_l n_l'(kR_{\rm WS})]}{j_l(kR_{\rm WS})-\tan\delta_l n_l(kR_{\rm WS})}\ , \tag{14}$$

where $j_l'(kR_{\rm WS})=[dj_l(x)/dx]_{x=kR_{\rm WS}}$ and $n_l'(kR_{\rm WS})=[dn_l(x)/dx]_{x=kR_{\rm WS}}$. Hence we can calculate phase shifts according to

$$\tan\delta_l=\frac{kj_l'(kR_{\rm WS})-\chi_l j_l(kR_{\rm WS})}{kn_l'(kR_{\rm WS})-\chi_l n_l(kR_{\rm WS})}\ . \tag{15}$$

Now, the scattering amplitude, $f(\theta)$, relates to the phase shift through[27,28]

$$f(\theta)=\frac{1}{2ik}\sum_{l=0}^{\infty}(2l+1)(e^{2i\delta_l}-1)P_l(\cos\theta)\ , \tag{16}$$

where θ is the polar scattering angle and $P_l(\cos\theta)$ is the Legendre polynomial of degree l. The elastic-scattering differential cross section is given by

$$\frac{d\sigma_e}{d\Omega}=|f(\theta)|^2\ , \tag{17}$$

where $d\Omega=2\pi\sin\theta\,d\theta$ is the differential solid angle in the direction of scattering electron.

B. Surface excitations

The differential probability per unit energy loss per unit momentum transfer that an electron excites a surface plasmon can be described in terms of the dielectric function of the solid. This probability was first derived by Ritchie[29] for normal incident electrons under the condition of neglecting the recoil effect. Neglecting the same effect, Raether[21] later worked out such a probability for obliquely incident electrons using the small-scattering-angle approximation. In this work, we consider the recoil effect without small-angle approximation. We find

$$P_s(\alpha,E\to E-\omega,\nu\to\nu-\mathbf{q})=\frac{|q_s|}{\pi^2\nu(\cos\alpha)q^4}\mathrm{Im}\left[\frac{(\epsilon-1)^2}{\epsilon(\epsilon+1)}\right]\times\delta\left[\omega-\nu\cdot\mathbf{q}+\frac{q^2}{2}\right] \quad (18)$$

for the differential probability of surface excitations by an electron of velocity ν and energy $E=\nu^2/2$ to lose energy ω and transfer momentum $\mathbf{q}$ to a solid surface. Here α is the angle between electron velocity and solid surface normal, q_s is the component of momentum transfer along the surface plane, and $\delta(\ )$ gives the energy-momentum conservation relation. We can decompose $\mathbf{q}$ into $q_\parallel$ and $q_\perp$, the parallel and perpendicular components along ν. Assuming the scattering angle θ lying on the plane of the incident electron, as sketched in Figs. 1(b) and 1(c), we can write

$$q_s=q_\perp\cos\alpha\pm q_\parallel\sin\alpha\ , \quad (19)$$

where the positive (negative) sign is for the same (opposite) signs of θ and α. Carrying out integrations over $\mathbf{q}$ and ω in Eq. (18), we obtain

$$P_s(\alpha,E)=P_{s+}(\alpha,E)+P_{s-}(\alpha,E)\ , \quad (20)$$

where

$$P_{s\pm}(\alpha,E)=\frac{1}{\pi\nu^2(\cos\alpha)}\int_0^E d\omega\int_{q_-}^{q_+}\frac{|q_s'|}{q^3}\mathrm{Im}\left[\frac{(\epsilon-1)^2}{\epsilon(\epsilon+1)}\right]dq \quad (21)$$

and

$$q_s'=\left[q^2-\left[\frac{\omega}{\nu}+\frac{q^2}{2\nu}\right]^2\right]^{1/2}\cos\alpha\pm\left[\frac{\omega}{\nu}+\frac{q^2}{2\nu}\right]\sin\alpha\ . \quad (22)$$

Since q_s' is different for positive and negative signs according to Eq. (22), an asymmetric effect exists in the surface excitation probability against scattering-angle orientations. This effect has been verified experimentally.[30–32]

If we neglect the recoil term in Eq. (18), Eq. (21) becomes

$$P_{s\pm}(\alpha,E)=\frac{1}{\pi\nu^2(\cos\alpha)}\int_0^E d\omega\int_{\omega/\nu}^{\infty}\frac{|q_s''|}{q^3}\mathrm{Im}\left[\frac{(\epsilon-1)^2}{\epsilon(\epsilon+1)}\right]dq \quad (23)$$

with

$$q_s''=\left[q^2-\left[\frac{\omega}{\nu}\right]^2\right]^{1/2}\cos\alpha\pm\frac{\omega}{\nu}\sin\alpha\ . \quad (24)$$

Ignoring the q dependence of the dielectric function, Eqs. (20) and (23) become

$$P_s(\alpha,E)=\frac{1}{\pi\nu^2(\cos\alpha)}\int_0^E\frac{\nu}{\omega}\left[\left[\frac{\pi}{2}-\alpha\right]\cos\alpha+\sin\alpha\right]\times\mathrm{Im}\left[\frac{(\epsilon-1)^2}{\epsilon(\epsilon+1)}\right]d\omega\ . \quad (25)$$

Substituting the free-electron-gas dielectric function into Eq. (25), we get

$$P_s(\alpha,E)=\frac{1}{2\nu}\frac{1}{\cos\alpha}\left[\left[\frac{\pi}{2}-\alpha\right]\cos\alpha+\sin\alpha\right]\ . \quad (26)$$

Taking $\alpha=0°$, we find that Eq. (26) reduces to the results of Ritchie[29] for normal incident electrons without recoil effect. Taking $\alpha=90°$, it shows that the surface excitation probability is proportional to $(\cos\alpha)^{-1}$. This angular dependence has been verified experimentally for large α values.[33] Note that Eq. (26) depends on electron energy and direction but not on material.

The function $P_s(\alpha,E)$ is actually the mean number of surface excitations. At glacing angles, say $\alpha\geq 80°$, it may approach or exceed unity.[21,34,35] This function approximates to the probability of a single-surface excitation if it is much less than unity. The occurrence of multiple-surface plasmons obeys the Poisson statistics.[35–38] Thus, the probability for an electron across the solid surface without generating surface plasmons is proportional to $\exp[-P_s(\alpha,E)]$.[21,34,36]

The dielectric function applied to Eq. (21) is the extended Drude function for the valence band of solids. This function is a generalization of the Drude function by allowing subbands of their own characteristic oscillator strengths, damping constants, and critical-point energies.[23] The real and imaginary parts of the dielectric function, in the limit of zero-momentum transfer, are given by[21–23]

$$\epsilon_1(0,\omega)=\epsilon_b-\sum_i\frac{A_i(\omega^2-\omega_i^2)}{(\omega^2-\omega_i^2)^2+(\omega\gamma_i)^2} \quad (27)$$

and

$$\epsilon_2(0,\omega)=\sum_i\frac{A_i\gamma_i\omega}{(\omega^2-\omega_i^2)^2+(\omega\gamma_i)^2}\ , \quad (28)$$

where A_i, γ_i, and ω_i are, respectively, the oscillator strength, damping constant, and critical-point energy, all associated with the ith subband. The inclusion of a background dielectric constant ϵ_b in Eq. (27) is to account for the influence of polarizable ion cores.[39] All these parameters are determined by a fit of Eq. (28) to the optical data measured experimentally. To ensure that the fitting results are accurate, we also require that sum rules are satisfied. Two sum rules are applied, i.e.,

$$\int_0^\infty\omega\epsilon_2(0,\omega)d\omega=\frac{\pi}{2}\sum_i A_i=\frac{\pi}{2}\omega_p^2 \quad (29)$$

and

$$\int_0^\infty\omega\,\mathrm{Im}\left[\frac{-1}{\epsilon(0,\omega)}\right]d\omega=\frac{\pi\omega_p^2}{2\epsilon_b^2}\ , \quad (30)$$

where ω_p is the plasma energy of valence electrons.

The extension of the dielectric function into the $q>0$ region, i.e., from $\epsilon(0,\omega)$ to $\epsilon(q,\omega)$, is established by substituting ω_i in Eqs. (27) and (28) by $\omega_i+q^2/2$.[40,41] This extension ensures the correctly asymptotic behavior of the dispersion relation at two extremes, i.e., the optical

end, $q \rightarrow 0$, and the Bethe ridge region, $q \rightarrow \infty$. The actual dispersion relation makes only minor difference in the determination of surface excitation probability.

C. Volume excitations

For an electron of energy E traveling in a homogeneous and isotropic solid, the inelastic mean free path, λ_i, for volume excitations of the valence band is given by[34,42]

$$\lambda_i^{-1}(E)=\frac{1}{\pi E}\int_0^E d\omega \int_{q_-}^{q_+}\frac{dq}{q}\mathrm{Im}\left[-\frac{1}{\epsilon(q,\omega)}\right], \quad (31)$$

where $q_\pm=\sqrt{2E}\pm\sqrt{2(E-\omega)}$ are derived from conservations of energy and momentum.

For inner-shell ionizations, we apply the local plasma approximation. This approximation has been proved useful in the treatment of inner-shell ionization cross sections.[43–46] Its contribution, however, is small for electron energies studied here.

IV. RESULTS AND DISCUSSION

Figure 2 shows a plot of elastic-scattering differential cross sections as a function of the scattering angle for electrons of several energies in Cu. The dashed and solid curves are, respectively, results corresponding to the TFD potential for free atoms[18] and the HFWS potential for solid atoms. It is seen that this cross section is larger for free atoms than for solid atoms at small scattering angles. This is because small-angle scatterings correspond to large impact parameters, where the screening of the nuclear charge is enhanced in solids. It is also seen that the cross section for backscatterings ($\theta > 90°$) is larger for lower energies. Thus, it leads to a greater intensity for elastically backscattered electrons of lower energies.

Table I lists values of parameters in the extended Drude dielectric function of Eqs. (27) and (28). These values were obtained by a fit of Eq. (28) in the long-wavelength limit to the optical data of Cu (Refs. 47–49)

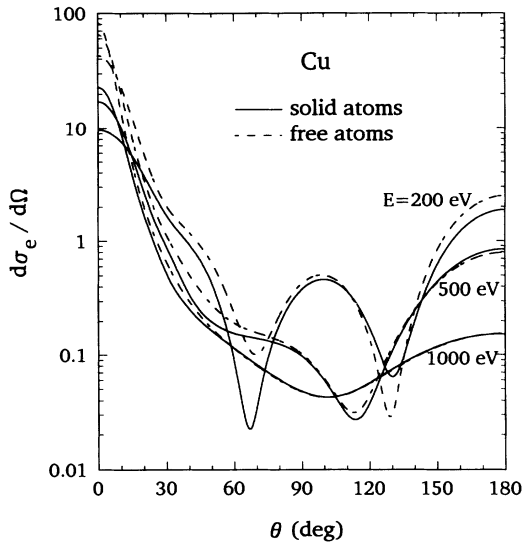

FIG. 2. Elastic-scattering differential cross section as a function of the scattering angle for electrons of several energies in Cu. The dashed and solid curves are, respectively, results calculated using the TFD potential for free atoms and the HFWS potential for solid atoms.

and Ag (Ref. 49). The fitting procedures involved a close check on $\epsilon_1(0,\omega)$, $\epsilon_2(0,\omega)$, $\mathrm{Im}[-1/\epsilon(0,\omega)]$, and sum rules of the latter two functions. In addition, the total valence oscillator strength, i.e., $\sum_i A_i$, also agreed with that calculated using observed plasmon energies.[21] Based on the model dielectric function, we have calculated the probability of surface excitations by electrons using Eqs. (20)–(22). Figure 3 shows the results of these calculations (solid curves) for normally incident electrons in Cu and Ag as a function of electron energy. Corresponding results of Ritchie[29] (dashed curve) are included in this figure for comparison. Note that Ritchie's results are independent on material owing to his over-simplified dielec-

TABLE I. Parameters in the model dielectric function of Eqs. (27) and (28) for Cu and Ag.

Cu $\epsilon_b=1.05$			Ag $\epsilon_b=1.03$		
A_i (eV^2)	γ_i (eV)	ω_i (eV)	A_i (eV^2)	γ_i (eV)	ω_i (eV)
64	0.03	0	80	0.07	0
6	0.3	0.3	4	0.45	4.8
6.5	0.65	2.5	10	1.2	5.3
5.5	0.7	3.1	20	2	6.4
4	0.7	3.7	240	11	15
55	2.6	5.05	70	5.38	22
42	4.76	8.93	160	15	31.3
172	10.18	14.74	300	36	40
80	8	25.6			
240	32	40			
90	30	55			
85	30	65			
200	25	83			
500	65	120			
664	160	200			

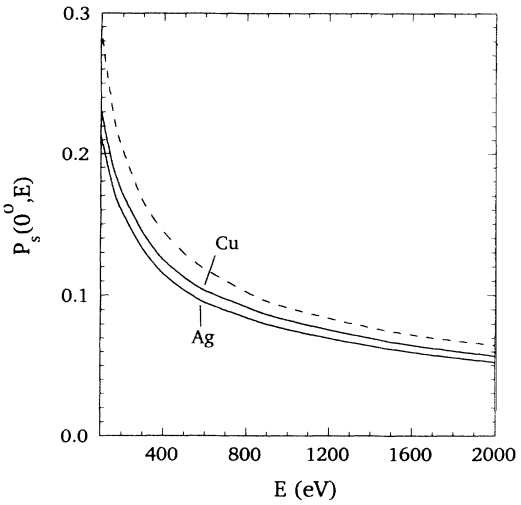

FIG. 3. The probability of surface excitations by normally incident electrons on Cu and Ag surfaces as a function of electron energy. The dashed and solid curves are, respectively, results of Ritchie's formulations (Ref. 29) and present calculations.

tric function. The neglect of recoil effect in Ritchie's formulation leads his results to higher values compared to present calculations. The increase in surface excitation probability for low-energy electrons is a consequence of the v^2 term in the denominator of Eq. (21). The monotonic increase of this probability with decreasing electron energy suggests that the contribution from surface excitations to elastically backscattered electrons is more important at low energies. Figure 4 shows a plot of the same probability as a function of the angle between electron velocity and solid surface normal, α, for 300-eV electron in Cu and Ag. Both results calculated using Eqs. (20)–(22) (solid curves) and Eq. (26) (dashed curve) are plotted for comparison. It shows that the recoil effect varies with the solid-electron angle. The sharp increase of surface excitation probability at large angles reveals that this excitation is most probable for glancing electrons. This confirms the experimental observations.[34]

Using the same dielectric function, we have calculated electron IMFP's for volume excitations using Eq. (31). Figure 5 shows a comparison of the results calculated presently (solid curve), by Penn (dashed curve),[19] and by Ashley and Tung (chain curve),[20] for electrons in Cu. The data of Ashley and Tung were based on a free-electron-gas statistical model incorporating the Hartree-Fock-Slater electron density distribution. Penn's calculations made use of a similar model but utilizing experimental optical data. Our calculations also applied experimental optical data but employed an extended Drude dielectric function rather than a single-pole free-electron-gas dielectric function used by Penn. A detailed discussion about the application of the extended Drude dielectric function to the calculation of electron IMFP's is given elsewhere.[23] The advantage of this function over the single-pole dielectric function lies in the region of very low energies (≤ 150 eV). Figure 5 shows that our results agree better with Penn's than with Ashley and Tung's data.

Inputting all cross-section data into a MC code, we have computed the elastic reflection coefficient and the angular distribution of electrons elastically backscattered from solid surfaces. Figure 6 shows the elastic reflection coefficient computed with (solid circles) and without (open circles) surface excitations and measured experimentally[50] (solid curve) for normally incident electrons backscattered from Cu surfaces into acceptance angles between 6° and 52°. The dashed curves represent interpolating results to guide the readers for easy comparison. It

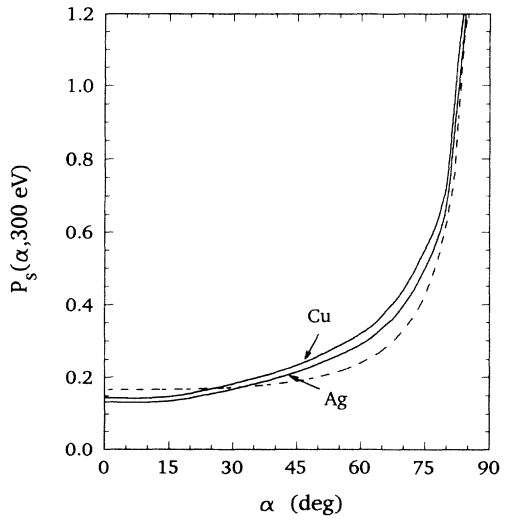

FIG. 4. The probability of surface excitations by 300-eV electrons incident on Cu and Ag surfaces as a function of the angle between electron velocity and solid surface normal. The dashed and solid curves are, respectively, results calculated using Eq. (26) and Eqs. (20)–(22).

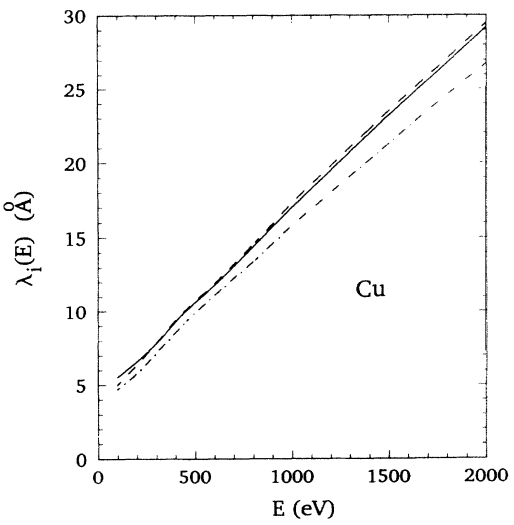

FIG. 5. A comparison of IMFP's for volume excitations calculated presently (solid curve), by Penn (dashed curve) (Ref. 19), and by Ashley and Tung (chain curve) (Ref. 20) for electrons in Cu.

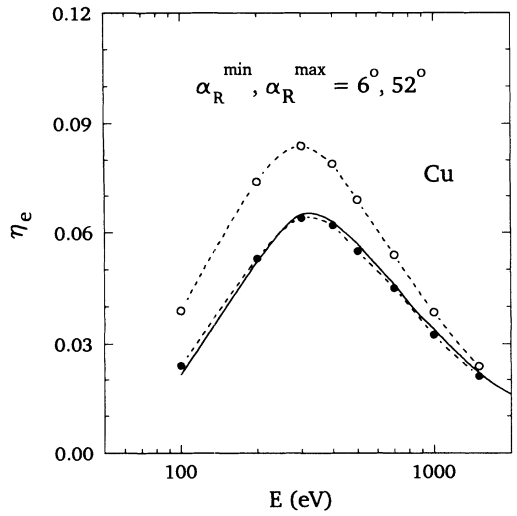

FIG. 6. A comparison of the elastic reflection coefficient computed presently with (solid circles) and without (open circles) surface excitations and measured experimentally (solid curve) (Ref. 50) for electrons in Cu. Results are for elastically backscattered electrons within acceptance angles between 6° and 52°. The dashed curves are interpolating results for guidance purpose.

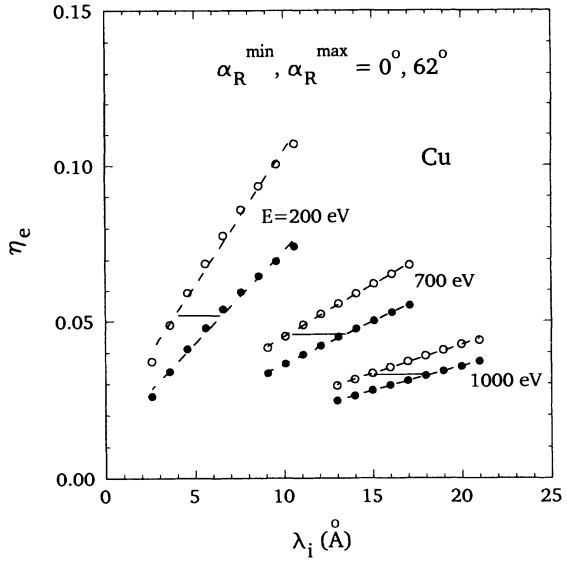

FIG. 8. A plot of the elastic reflection coefficient computed presently with (solid circles) and without (open circles) surface excitations as a function of IMFP for electrons in Cu. The dashed curves are interpolating results for guidance purpose. The horizontal solid lines represent data measured experimentally (Ref. 50). Results are for elastically backscattered electrons within acceptance angles between 0° and 62°.

shows that present results including surface excitations agree very well with experimental data at all electron energies. The contribution from surface excitations to the elastic reflection coefficient is significant for electron energies below several hundred eV. Theoretical results of Jablonski *et al.*,[14] who neglected surface excitations and used different elastic and volume excitation cross sections, lie somewhat below the open circle curve. A similar plot of the elastic reflection coefficient for electrons backscattered from Ag surfaces is shown in Fig. 7. Here again present results including surface excitations agree closely with experimental data.

Using elastic reflection coefficient data, one may extract electron IMFP's. To do this, we treat IMFP as a

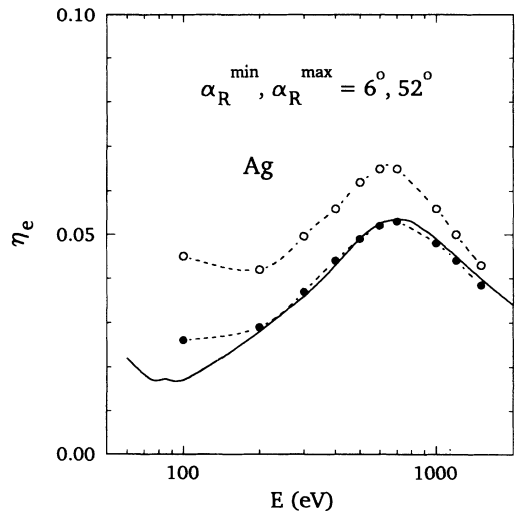

FIG. 7. A comparison of the elastic reflection coefficient computed presently with (solid circles) and without (open circles) surface excitations and measured experimentally (solid curve) (Ref. 50) for electrons in Ag. Results are for elastically backscattered electrons within acceptance angles between 6° and 52°. The dashed curves are interpolating results for guidance purpose.

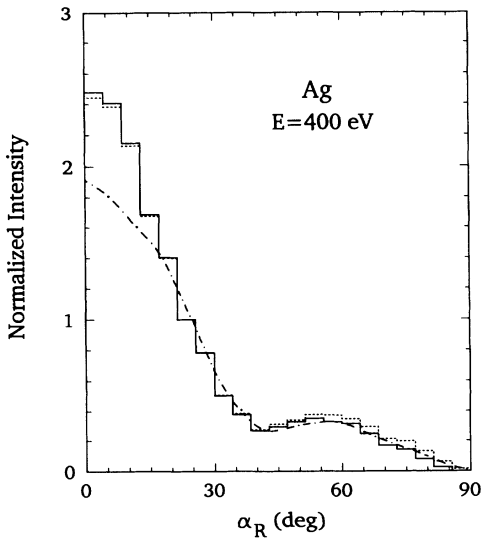

FIG. 9. A comparison of the angular distribution of elastically backscattered electrons computed presently with (solid histogram) and without (dashed histogram) surface excitations and measured experimentally (chain curve) (Ref. 51) for 400-eV electrons in Ag. The results are normalized to the backscattered electron intensity of 25° escape angle.

variable instead of inputting a fixed value into the MC code. Figure 8 shows a plot of elastic reflection coefficients computed with (solid circles) and without (open circles) surface excitations as a function IMFP for electrons of several energies in Cu. Applying experimentally measured elastic reflection coefficients (horizontal solid lines), one can determine the correct IMFP data from the intersections of solid lines and solid circles. It reveals that excellent agreement is found between these data and the IMFP's shown in Fig. 5.

Finally, we compare the angular distribution of elastically backscattered electrons computed with (solid histogram) and without (dashed histogram) surface excitations and determined experimentally (chain curve).[51] Figure 9 shows such a comparison for 400-eV electrons normally incident on Ag surfaces. Note that all results are normalized to the backscattered electron intensity at a 25° escape angle. It is seen that the influence of surface excitations is relatively more important at larger escape angles due to the increased surface excitation probability at these angles, as shown in Fig. 4. It is also seen that this influence on angular distribution of elastically backscattered electrons is not as prominent as on elastic reflection coefficient. It should be pointed out that experimental data at small angles (0°–25°) were not measured but extrapolated from larger angles. Our results at small angles indicate that these extrapolated values might underestimate the elastically backscattered electrons.

V. CONCLUSIONS

Monte Carlo calculations have been performed for studies of the influence of surface excitations on the elastic backscattering of electrons from solid surfaces. These calculations showed that such an influence on the elastic reflection coefficient was significant for low-energy electrons. The influence on the angular distribution of elastically backscattered electrons was less significant and only important for large escape angles. Results of present calculations are in good agreement with experimental data.

It is worthwhile to mention that present theory is applicable to polycrystalline and amorphous solids only. For single crystals, the diffraction effect focuses the electron beam to a certain direction depending on the orientation of crystals. This effect diminishes in polycrystalline and amorphous solids due to the random elastic scatterings, which defocus the electron beam.[11,34]

ACKNOWLEDGMENT

This research was supported by the National Science Council of the Republic of China under Contract No. NSC83-0404-E-009-065.

[1]J. Kirschner and P. Staib, Phys. Lett. **42**, 335 (1973).
[2]J. Kirschner and P. Staib, Appl. Phys. **6**, 99 (1975).
[3]G. Gergely, Surf. Interface Anal. **3**, 201 (1986).
[4]A. Jablonski, Surf. Sci. **151**, 166 (1985).
[5]G. Gergely, Scanning **8**, 203 (1986).
[6]B. Gruzza, B. Achad, and C. Pariset, J. Phys. D **19**, 137 (1986).
[7]W. Donlinski, S. Mróz, and M. Zagórski, Surf. Sci. **200**, 361 (1988).
[8]B. Lesiak, A. Jablonski, Z. Prussak, and P. Mrozek, Surf. Sci. **223**, 213 (1989).
[9]B. Gruzza and C. Pariset, Surf. Sci. **247**, 408 (1991).
[10]C. Jardin, G. Gergely, and B. Gruzza, Surf. Interface Anal. **19**, 5 (1992).
[11]S. Touggard and I. Chorkendorff, Phys. Rev. B **35**, 6570 (1987).
[12]S. Touggard and J. Kraaer, Phys. Rev. B **43**, 1651 (1991).
[13]C. J. Tung, Y. F. Chen, C. M. Kwei, and T. L. Chou, Phys. Rev. B **49**, 16 684 (1994).
[14]A. Jablonski, J. Gryko, J. Kraaer, and S. Touggard, Phys. Rev. B **39**, 61 (1989).
[15]A. Jablonski, Phys. Rev. B **43**, 7546 (1991).
[16]A. Jablonski, H. S. Hansen, C. Jansson, and S. Touggard, Phys. Rev. B **45**, 3694 (1992).
[17]A. Jablonski, C. Jasson, and S. Touggard, Phys. Rev. B **47**, 7420 (1993).
[18]R. A. Bonham and T. G. Strand, J. Chem. Phys. **39**, 2200 (1963).
[19]D. R. Penn, Phys. Rev. B **35**, 482 (1987).
[20]J. C. Ashley and C. J. Tung, Surf. Interface Anal. **4**, 52 (1982).
[21]H. Raether, in *Excitations of Plasmons and Interband Transitions by Electrons,* edited by G. Höhler, Springer Tracts in Modern Physics Vol. 88 (Springer, New York, 1980).
[22]R. H. Ritchie and A. Howie, Philos. Mag. **36**, 463 (1977).
[23]C. M. Kwei, Y. F. Chen, C. J. Tung, and J. P. Wang, Surf. Sci. **293**, 202 (1993).
[24]L. Reimer, in *Scanning Electron Microscopy,* edited by P. W. Hawkes, Springer Tracts in Optical Sciences Vol. 45 (Springer, New York, 1985), p. 114.
[25]R. Schimizu, Y. Kataoka, T. Ikuta, T. Koshikawa, and H. Hashimoto, J. Phys. D **9**, 101 (1976).
[26]T. C. Tucker, L. D. Roberts, C. W. Nestor, and T. A. Carson, Phys. Rev. **178**, 998 (1969).
[27]C. J. Jochain, *Quantum Collision Theory* (North-Holland, Amsterdam, 1975).
[28]F. Salvat, R. Mayol, E. Molins, and J. Parallada, J. Phys. D **18**, 1404 (1985).
[29]R. H. Ritchie, Phys. Rev. **106**, 874 (1957).
[30]C. Kunz, Z. Phys. **180**, 127 (1964).
[31]M. Creuzburg, Z. Phys. **174**, 511 (1963).
[32]R. B. Pettit, J. Silicox, and R. Vincent, Phys. Rev. B **11**, 3116 (1975).
[33]C. J. Powell, Phys. Rev. **175**, 972 (1968).
[34]R. F. Egerton, *Electron Energy-Loss Spectroscopy in the Electron Microscope* (Plenum, New York, 1986).
[35]A. A. Lucas, Phys. Rev. Lett. **26**, 229 (1971).
[36]E. Evans and D. L. Mills, Phys. Rev. B **5**, 4126 (1972).
[37]E. Evans and D. L. Mills, Phys. Rev. B **7**, 853 (1973).
[38]J. Schilling, Z. Phys. B **25**, 61 (1976).
[39]D. Y. Smith and E. Shiles, Phys. Rev. B **17**, 4689 (1978).
[40]R. H. Ritchie, R. N. Hamm, J. E. Turner, H. A. Wright, and W. E. Bolch, in *Physical and Chemical Mechanisms in Molecular Radiation Biology,* edited by W. A. Glass and M. N. Varma (Plenum, New York, 1991), p. 99.
[41]C. J. Tung and C. Lin, Radiat. Effects **80**, 261 (1984).

[42]C. J. Tung and R. H. Ritchie, Phys. Rev. B **16**, 4302 (1977).
[43]J. Lindhard and M. Scharff, K. Dan. Vidensk. Selk. Mat. Fys. Medd. **27**, 1 (1953).
[44]W. K. Chu and D. Powers, Phys. Lett. **40A**, 23 (1972).
[45]C. J. Tung and C. M. Kwei, Nucl. Instrum. Methods B **12**, 464 (1985).
[46]C. M. Kwie and C. J. Tung, J. Phys. D **19**, 255 (1986).
[47]B. Dold and R. Mecke, Optik **22**, 435 (1965).
[48]H. J. Hagemann, W. Gudat, and C. Kunz, J. Opt. Soc. Am. **65**, 472 (1975).
[49]D. W. Lynch and W. R. Hunter, in *Handbook of Optical Constants of Solids I,* edited by E. D. Palik (Academic, New York, 1985), p. 275.
[50]R. Schmid, K. H. Gaukler, and H. Seiler, in *Scanning Electron Microscopy,* edited by O. Johari (SEM, Chicago, 1983), Vol. II, p. 501.
[51]M. Bronshtein and V. P. Pronin, Fiz. Tverd. Tela (Leningrad) **17**, 2086 (1975) [Sov. Phys. Solid State **17**, 1363 (1976)].